Electrochemistry Studies of $[Ir(\mu\text{-pz})(COD)]_2$ in Halocarbon and Acetonitrile Solutions. Solvent Control of Sequential Electron-Transfer Thermodynamics

David C. Boyd, Gary S. Rodman, and Kent R. Mann*

Contribution from the Department of Chemistry, University of Minnesota, Minneapolis, Minnesota 55455. *Received September 3, 1985*

Abstract: Electrochemical studies of $[Ir(\mu\text{-pz})(COD)]_2$ (μ-pz = bridging pyrazolyl, COD = 1,5-cyclooctadiene) in halocarbon and CH_3CN solutions have been completed. In CH_2Cl_2 solutions, the cyclic voltammogram (CV) of $[Ir(\mu\text{-pz})(COD)]_2$ exhibits two, thermodynamically distinct one-electron oxidations. The first oxidation is quasi-reversible ($E^{\circ\prime}_{1/0}$ = +0.424 in CH_2Cl_2/TBAH; TBAH = tetra-*n*-butylammonium hexafluorophosphate). $E^{\circ\prime}_{1/0}$ is nearly independent of supporting anion (PF_6^-, ClO_4^-, and AsF_6^-). The second oxidation is chemically irreversible. The position of $E_{p,a}$ for the second oxidation is variable due to complexation of $[Ir(\mu\text{-pz})(COD)]_2^{2+}$ with the supporting anion. $E_{p,a}$ occurs at +0.963, +1.280, and +1.383 V with ClO_4^-, PF_6^-, and AsF_6^- as the supporting anion. Bulk electrolysis at potentials positive of the quasi-reversible oxidation results in the removal of 2.0 (1) electrons. A slow reaction on the CV time scale occurs between $[Ir(\mu\text{-pz})(COD)]_2^+$ and CH_2Cl_2 to form an $Ir^{II}Ir^{II}$-containing product. The addition of CH_3CN to CH_2Cl_2 solutions of $[Ir(\mu\text{-pz})(COD)]_2$ causes the second electrode process to shift to less positive potentials. The first wave does not shift. At $[CH_3CN] \approx 2.0$ M, the second wave merges with the first to give a single feature that corresponds to a net two-electron process. The wave corresponding to this two-electron process also shifts toward negative potentials with increasing $[CH_3CN]$. In neat CH_3CN/TBAH solutions, the two-electron oxidation process occurs at +0.262 V. Bulk electrolysis in neat CH_3CN solutions at potentials positive of the 2-electron process results in the removal of 2.0 (1) electrons. The observed shifts in electron-transfer thermodynamics arise from the strong complexation of two CH_3CN ligands with the two-electron oxidized $[Ir(\mu\text{-pz})(COD)]_2^{2+}$ complex. The potential for net two-electron-transfer chemistry from the lowest excited state of $[Ir(\mu\text{-pz})(COD)]_2$ is discussed in terms of a modified Latimer diagram.

In recent years, we have been interested in the photophysics, photochemistry, and electrochemistry of binuclear transition-metal complexes that contain d^8–d^8 chromophores.[1-9] The major thrust of these investigations has been to design and study systems that are capable of excited state multielectron-transfer reactions.

Electrochemical studies[8b] of a Rh^IRh^I system, $Rh_2(dimen)_4^{2+}$ (dimen = 1,8-diisocyanomenthane), have indicated that the ground state is in equilibrium with the two-electron oxidized form at glassy carbon electrodes. The removal of the second electron is thermodynamically more favorable than the first due to large increases in the strength of Rh–Rh and axial Rh–L bonding in the $Rh^{II}Rh^{II}$ state relative to the $Rh^{I(1/2)}Rh^{I(1/2)}$ state.

In homogeneous solutions, $[Ir(\mu\text{-pz})(COD)]_2$ (μ-pz = bridging pyrazolyl, COD = 1,5-cyclooctadiene) exhibits oxidation chemistry similar to that of $Rh_2(dimen)_4^{2+}$ and other $Rh_2(diisocyanoalkane)_4^{2+}$ cations. Excitation of the binuclear species in 1,2-dichloroethane (DCE) or dichloromethane yields net two-electron oxidation of the Ir^IIr^I core with concomitant addition of one ligand to each resulting Ir^{II} center and the formation of an $Ir^{II}Ir^{II}$ bond.[10] These reactions were suggested to occur through the intermediacy of odd-electron species that form and subsequently collapse to products during the lifetime of a solvent cage.

We now report the results of electrochemical studies that indicate that $[Ir(\mu\text{-pz})(COD)]_2$ is capable of both thermodynamically distinguishable one-electron-transfer reactions, and, under different experimental conditions, a single, net two-electron process stabilized by $Ir^{II}Ir^{II}$ and Ir^{II}–L bond formation.

Experimental Section

Synthesis. $[Ir(\mu\text{-pz})(COD)]_2$ (μ-pz = bridging pyrazolyl, COD = 1,5-cyclooctadiene) was synthesized by the method of Stobart et al.[11]

Electrochemical Measurements. All electrochemical experiments were performed with a BAS 100 electrochemical analyzer.

Cyclic voltammetry (CV) and chronocoulometry (CC) were performed at 20 ± 2 °C with a normal three-electrode configuration consisting of a highly polished glassy-carbon-disk working electrode (A = 0.07 cm^2) and a AgCl/Ag reference electrode containing 1.0 M KCl. The working compartment of the electrochemical cell was separated from the reference compartment by a modified Luggin capillary. All three compartments contained a 0.1 M solution of the supporting electrolyte.

Table I. Potentials Measured for the Oxidations of $[Ir(\mu\text{-pz})(COD)]_2$ and $FeCp_2$ in Halocarbon Solutions as a Function of Supporting Electrolyte

solvent/supporting anion	$E^{\circ\prime}_{1/0}$ [a]	$E_{p,a}$ [b]	$E_{p,c}$ [c]	$FeCp_2^+/FeCp_2$ [d]
$CH_2Cl_2/TBA^+ClO_4^-$	+0.473	+0.963	+0.849	+0.505
$CH_2Cl_2/TBA^+PF_6^-$	+0.424	+1.280		+0.460
$CH_2Cl_2/TBA^+PF_6^-$	+0.428	+1.185	+1.080	+0.470
$CH_2Cl_2/TBA^+AsF_6^-$	+0.420	+1.383		+0.447

[a] Formal potential for the $[Ir(\mu\text{-pz})(COD)]_2^+/[Ir(\mu\text{-pz})(COD)]_2$ couple. [b] Anodic peak potential for the oxidation of $[Ir(\mu\text{-pz})(COD)]_2^+$ to $[Ir(\mu\text{-pz})(COD)]_2^{2+}$. [c] Cathodic return peak potential for the reduction of $[Ir(\mu\text{-pz})(COD)]_2^{2+}$ to $[Ir(\mu\text{-pz})(COD)]_2^+$. [d] Observed potential for the $FeCl_2^+/FeCp_2$ couple.

Bulk electrolyses were performed by substituting a Pt-mesh electrode for the glassy carbon electrode in the cell described above. Linear sweep voltammetry (LSV) was utilized with a pyrolytic graphite rotating disk electrode (RDE) (Pine Instruments) of area 0.53 cm^2 to obtain the characteristic i vs. E curves under various experimental conditions.

The acetonitrile, dichloromethane, 1,2-dichloroethane (Burdick & Jackson), and supporting electrolytes tetrabutylammonium hexafluoro-

* To whom correspondence should be addressed.

(1) Mann, K. R.; Lewis, N. S.; Miskowski, V. M.; Erwin, D. K.; Hammond, G. S.; Gray, H. B. *J. Am. Chem. Soc.* **1977**, *99*, 5525.
(2) Miskowski, V. M.; Mann, K. R.; Gray, H. B.; Milder, S. J.; Hammond, G. S.; Ryason, P. R. *J. Am. Chem. Soc.* **1979**, *101*, 4383.
(3) Gray, H. B.; Miskowski, V. M.; Milder, S. J.; Smith, T. P.; Maverick, A. W.; Buhr, J. D.; Gladfelter, W. L.; Sigal, I. S.; Mann, K. R. *Fundamental Research on Homogeneous Catalysis*; Tsutusi, M., Ed., Plenum: New York, 1979; Vol. 3, p 819.
(4) Gray, H. B.; Mann, K. R.; Lewis, N. S.; Thich, J. A.; Richman, R. M. *Adv. Chem. Ser.* **1978**, *168*, 44.
(5) Miskowski, V. M.; Nobinger, G. L.; Kliger, K. S.; Hammond, G. S.; Lewis, N. S.; Mann, K. R.; Gray, H. B. *J. Am. Chem. Soc.* **1978**, *100*, 485.
(6) Mann, K. R.; Gray, H. B. *Adv. Chem. Ser.* **1979**, *173*, 226.
(7) Mann, K. R.; Parkinson, B. A. *Inorg. Chem.* **1981**, *20*, 1921.
(8) (a) Womack, D. R.; Enlow, P. D.; Woods, C. *Inorg. Chem.* **1983**, *22*, 2653. (b) Rhodes, M. R.; Mann, K. R. *Inorg. Chem.* **1984**, *23*, 2053. (c) Enlow, P. D.; Woods, C. *Inorg. Chem.* **1985**, *24*, 1273.
(9) Rodman, G. S.; Mann, K. R. *Inorg. Chem.* **1985**, *24*, 3507.
(10) Caspar, J. V.; Gray, H. B. *J. Am. Chem. Soc.* **1984**, *106*, 3029.
(11) Coleman, A. W.; Eadie, D. T.; Stobart, S. R.; Zaworotko, M. J.; Atwood, J. L. *J. Am. Chem. Soc.* **1982**, *104*, 922.

0002-7863/86/1508-1779$01.50/0

phosphate (TBAH), tetrabutylammonium perchlorate (TBAP) (Southwestern Analytical Chemicals, Inc.), and tetrabutylammonium hexafluoroarsenate (TBAHA)[12] were used without further purification.

Electrolyte solutions were prepared and stored over 80–200-mesh activated alumina (Fisher Scientific Co.) or activated 4-Å molecular sieves prior to use in the experiments. In all cases, working solutions were prepared by recording background cyclic voltammograms of 25.0 mL of the electrolyte solution before addition of the complex. The working compartment of the cell was bubbled with solvent-saturated argon to deaerate the solution.

Potentials are reported vs. aqueous AgCl/Ag and are not corrected for the junction potential. To allow future corrections and the correlation of these data with those of other workers, we have measured the $E^{\circ\prime}$ for the ferrocenium/ferrocene couple[13] under conditions identical with those used for the Ir complex. These values are given in Table I. In CH_3CN/TBAH, $E^{\circ\prime} = +0.410$ V. The standard current convention is used (anodic currents are negative).

The iR compensation circuit available on the BAS-100 was not used in any of the electrochemical studies. Rather, the effects of uncompensated cell resistance were assessed for the LSV studies at the RDE by determining the LSV response for $FeCp_2$. The slopes of the E vs. $\log\{(i_{c,l} - i)/(i - i_{a,l})\}$ plots[14] for the oxidation of $FeCp_2$ were 0.092 and 0.067 V for CH_2Cl_2/TBAH and CH_3CN/TBAH solutions, respectively.

Data Handling. Digital data collected on the BAS-100 electrochemical system were down loaded to a Zenith-150 microcomputer. All data analyses were performed by utilizing the commercially available LOTUS-123 computer program.

Sequential Additions of CH_3CN. Sequential additions of neat CH_3CN/TBAH, 0.76 or 1.9 M CH_3CN/TBAH in CH_2Cl_2/TBAH, were made with a microliter syringe. Analysis of the data assumed that the quasi-reversible CV waves observed for the various conditions studied approximated true Nernstian conditions. We believe that the successful fitting of experimental data to predicted linear relationships justifies this assumption.

Case A. (The cases are summarized in Table II.) Data were analyzed by using

$$\log([\text{complexed}]/[\text{uncomplexed}]) = p \log [CH_3CN] + \log K_1 \quad (1)$$

where

$$\log([\text{complexed}]/[\text{uncomplexed}] \approx \log(i_a)/(i_{a,l} - i_a)] \quad (2)$$

$$\log [CH_3CN] = \log([CH_3CN]_{added} - p[\text{complexed}]) \quad (3)$$

$i_{a,l}$ = limiting anodic peak current for the oxidation of $[Ir(\mu\text{-pz}) = (COD)]_2^+$ that grows in when CH_3CN is added (CV experiment; $\nu = 100$ mV/s)

i_a = anodic peak current at a given CH_3CN concentration

$$[\text{complexed}] = [[Ir(\mu\text{-pz})(COD)]_2(CH_3CN)_p^{2+}]$$

$$[\text{uncomplexed}] = [[Ir(\mu\text{-pz})(COD)]_2^{2+}]$$

$$K_1 = \frac{[[Ir(\mu\text{-pz})(COD)]_2(CH_3CN)_p^{2+}]}{[[Ir(\mu\text{-pz})(COD)]_2^{2+}][CH_3CN]^p} \quad (4)$$

Case B. Data were analyzed by using eq 5[15] where $E_{p,a}$ is the anodic peak potential for the second oxidation wave, $E_{2/1}{}^{\circ\prime}$ is the formal potential for the reverse of eq 7, K_1K_2 is the overall formation constant for equilbrium 21, and q is the total number of CH_3CN ligands bound by the two-electron oxidized form.

$$E_{p,a} = E_{2/1}{}^{\circ\prime} - (2.303RT/nF)\{\log K_1K_2 + q \log [CH_3CN]\} + (\Delta E_{solvation} + \Delta E_{junction} + 0.029) \quad (5)$$

The next two ΔE terms in eq 5 are contributions to the intercept that arise from changes in solvation energy and junction potential. The last term corrects the right side of the equation to correspond to the anodic peak potential. All diffusion coefficients for Ir-containing species are assumed to be identical, and complexation of CH_3CN by the one-electron oxidized form is assumed negligible (see Results and Discussion section).

Table II. Summary of $[Ir(\mu\text{-pz})(COD)]_2$ CV Behavior in CH_2Cl_2/CH_3CN Mixtures

case	solution characteristics	CV characteristics
A	$[CH_3CN]/[[Ir(\mu\text{-pz})(COD)]_2] \leq 2$; $0 < [CH_3CN] < 10$ mM; $[Ir(\mu\text{-pz})(COD)]_2 \approx 5$ mM	three waves; $E^{\circ\prime}_{1/0}$ independent of $[CH_3CN]$; $E_{p,a}$ at 1.28 V gradually disappears while the current of $E_{p,a}$ at +0.849 V gradually increases with an increase in $[CH_3CN]$
B	$[CH_3CN]/[[Ir(\mu\text{-pz})(COD)]_2] > 2$; $[[Ir(\mu\text{-pz})(COD)]_2] = 0.5$ mM; $[CH_3CN] < 0.2$ M	two quasi-reversible waves; $E^{\circ\prime}_{1/0}$ independent of $[CH_3CN]$; $E_{2/1}$ shifts to less positive potentials with an increase in $[CH_3CN]$
C	$[CH_3CN]/[[Ir(\mu\text{-pz})(COD)]_2] \gg 2$; $[[Ir(\mu\text{-pz})(COD)]_2] = 0.5$ mM; 2.0 M $< [CH_3CN] <$ 19.9 M	single $2e^-$ wave; the wave gradually shifts to less positive potentials with an increase in $[CH_3CN]$

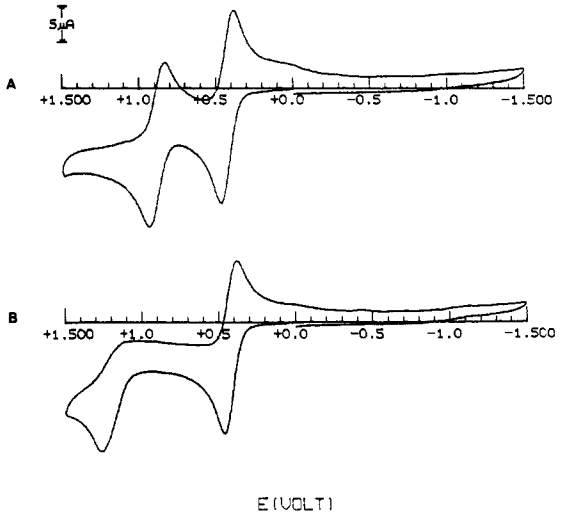

Figure 1. Cyclic voltammograms ($\nu = 100$ mV/s) at a stationary glassy carbon electrode of 0.80 mM $[Ir(\mu\text{-pz})(COD)]_2$ in CH_2Cl_2/TBAH. Curve A results from "moist" conditions; curve B results after addition of activated 4-Å molecular sieves followed by 5 min of stirring.

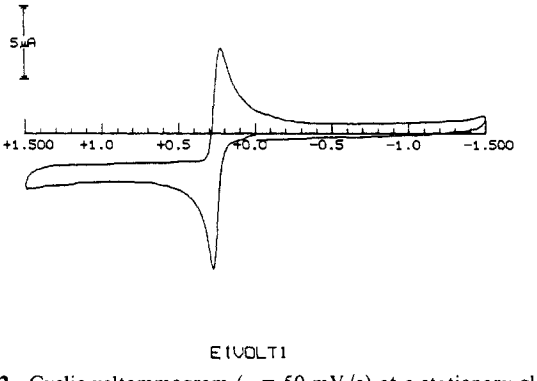

Figure 2. Cyclic voltammogram ($\nu = 50$ mV/s) at a stationary glassy carbon electrode of 0.27 mM $[Ir(\mu\text{-pz})(COD)]_2$ in CH_3CN/TBAH.

Results and Discussion

The cyclic voltammograms of $[Ir(\mu\text{-pz})(COD)]_2$ in dry CH_2Cl_2/TBAH (TBAH = tetra-*n*-butylammonium hexafluorophosphate) and CH_3CN/TBAH are shown in Figures 1B and 2, respectively.

(12) Schrenk, J. L.; Palazzotto, M. C.; Mann, K. R. *Inorg. Chem.* **1983**, *22*, 4047.

(13) (a) Gagne, R. R.; Koval, C. A.; Kisensky, G. C. *Inorg. Chem.* **1980**, *19*, 2854. (b) Koepp, H. M.; Wendt, H.; Strehlow, H. Z. *Z. Elektrochem.* **1960**, *64*, 483.

(14) Bard, A. J.; Faulkner, L. R. *Electrochemical Methods*; Wiley: New York, 1980; p 290.

(15) This equation is a more specific version of one used previously to analyze similar data: Kadish, K. M.; Bottomley, L. A.; Cheng, J. S. *J. Am. Chem. Soc.* **1978**, *100*, 2731.

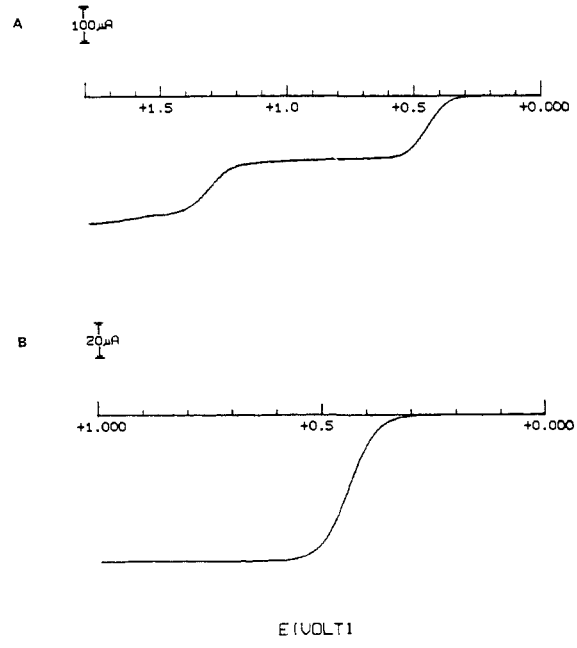

Figure 3. (A) Plot of the LSV (current (i) vs. potential (E)) at a pyrolytic graphite RDE (ω = 52.36 rad/s; ν = 20 mV/s) of a 0.83 mM solution of $[Ir(\mu\text{-pz})(COD)]_2$ in CH_2Cl_2/TBAH. (B) Plot of the LSV (current (i) vs. potential (E)) at a pyrolytic graphite RDE (ω = 10.47 rad/s; ν = 1 mV/s) of a 0.27 mM solution of $[Ir(\mu\text{-pz})(COD)]_2$ in CH_3CN/TBAH.

Two oxidation processes are observed in the CH_2Cl_2 solution, while a single process is observed in CH_3CN solutions. The behavior of $[Ir(\mu\text{-pz})(COD)]_2$ in CH_2Cl_2 solutions will be discussed first.

$[Ir(\mu\text{-pz})(COD)]_2$ in CH_2Cl_2 Solutions. In carefully dried CH_2Cl_2/TBAH solutions, two oxidative electrode processes occur between 0.0 V and the solvent limit (~2.0 V). The first process occurs at +0.424 V and corresponds to a one-electron process ($i_{p,c}/i_{p,a}$ = 1.00 ± 0.02, ΔE_p = 148 mV at ν = 100 mV/s). A potential step experiment from 0.0 to 0.8 V yielded a linear (correlation coefficient = 0.9999) Anson plot (Q vs. $t^{1/2}$)[16] with a slope of 29.6 $C/s^{1/2}$ for 1.22 mM $[Ir(\mu\text{-pz})(COD)]_2$. From the slope, a value of $nD^{1/2}$ of 3.19×10^{-3} $cm/s^{1/2}$ was obtained. A calculation[17] of the diffusion coefficient from the molecular volume and the Stokes–Einstein equation gave $D = 1.03 \times 10^{-5}$ cm^2/s, in excellent agreement with the experimentally determined value $D = 1.02 \times 10^{-5}$ cm^2/s if n is assumed to be 1.

As a further indication of the nature of the electrode process, the LSV was obtained at the RDE with ν = 1 mV/s and ω = 10.47 rad/s (Figure 3A). The plot of E vs. log $[i_{c,1} - i)/(i - i_{a,1})]$ (where $i_{c,1}$ and $i_{a,1}$ are the limiting cathodic and anodic currents, respectively)[14] shown in Figure 4 is linear and yields an intercept ($E^{\circ\prime}$) of +0.439 V and a slope of 0.072 V. The deviation of the slope from the 0.057 V expected for a perfectly Nernstian system is consistent with some uncompensated cell resistance and the value of 0.092 V determined for the $FeCp_2^{+/0}$ couple under identical conditions. All of the data are consistent with a quasi-reversible, one-electron designation for this electrode process.

Bulk electrolysis at +0.6 V (positive of the first one-electron process) of carefully dried solutions of $[Ir(\mu\text{-pz})(COD)]_2$ in either CH_2Cl_2/TBAH or CH_2Cl_2/TBAP gave an n value of 2.0 and resulted in the formation of red solutions. CV's of these solutions

(16) Bard, A. J.; Faulkner, L. R. *Electrochemical Methods*; Wiley: New York, 1980; p 200.

(17) Calculated values for the diffusion coefficients of $[Ir(\mu\text{-pz})(COD)]_2$ were obtained from the Stokes–Einstein equation: D (cm^2/s) = (1×10^7)-$(RT/6\pi rN\eta)$ where R = gas constant, T = absolute temperature, r = molecular radius (cm), η = solvent viscosity (P), and N = Avogadro's number. The molecular radius, r, was estimated to be 4.967×10^{-8} cm based on the observed molecular volume taken from crystal structure data in ref 11. Viscosity values of 4.21×10^{-3} and 3.45×10^{-3} P for CH_2Cl_2 and CH_3CN were employed.

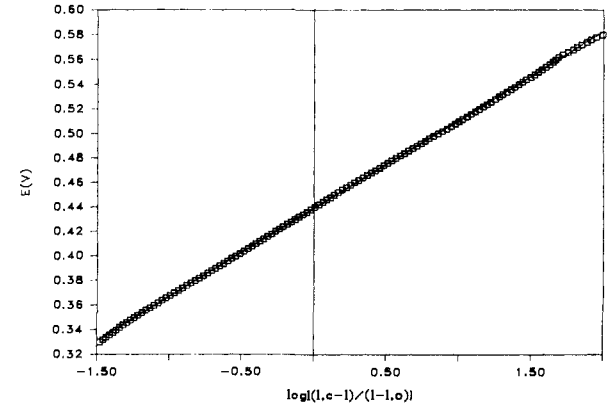

Figure 4. Plot of potential (E) vs. log $[(i_{c,1} - i)/(i - i_{a,1})]$ for the first oxidative electrode process exhibited by a 0.75 mM solution of $[Ir(\mu\text{-pz})(COD)]_2$ in CH_2Cl_2/TBAH. $i_{c,1}$ and $i_{a,1}$ are the limiting cathodic and anodic currents observed in the LSV (Figure 3A) obtained at a pyrolytic graphite RDE with ω = 10.47 rad/s and ν = 1 mV/s. Experimental points are presented as squares. The least-squares line has slope = +0.072 V and intercept = +0.439 V.

after electrolysis indicated that a chemical reaction, slow on the CV time scale, had occurred to produce an $Ir^{II}Ir^{II}$ compound. The electronic spectrum of this species produced by bulk electrolysis at potentials positive of the n = 1 electrode process is nearly identical with the published electronic spectrum of the CH_2Cl_2 oxidative addition product, $[Ir(\mu\text{-pz})(COD)]_2(CH_2Cl)(Cl)$.[10]

The formation of a *two*-electron, oxidative addition product from the $[Ir(\mu\text{-pz})(COD)]_2^+$ species formed via the n = 1 electrode reaction may have mechanistic implications in the previously studied photochemical oxidative addition of CH_2Cl_2 to $[Ir(\mu\text{-pz})(COD)]_2$.[10] More detailed studies to determine the organic products and the mechanism of this reaction under electrochemical conditions will be reported in a separate study.

The second electrode process that occurs at $E_{p,a}$ = +1.28 V ($E_{p,a}$ is the anodic peak potential) in CH_2Cl_2/TBAH solution is *not* chemically reversible ($i_{p,c}/i_{p,a} \approx 0$ at ν = 100 mV/s) but again corresponds to a one-electron electrode process on the CV time scale. A potential step from 0.0 to +1.5 V across both one-electron oxidations yields an Anson plot with a slope of 59.9 $C/s^{1/2}$, 2.02 times that observed for the 0.0 to +0.8 V step across only the first wave. The analysis of the LSV–RDE curve gives a linear plot of E vs. log $\{(i_{c,1} - i)/(i - i_{a,1})\}$ with slope = +0.096 V and intercept of +1.26 V.

Some degree of chemical irreversibility in the electrochemical response of other d^8–d^8 systems has been previously noted.[8] As before, the chemical irreversibility is due to the rapid addition of solvent molecules or supporting anions to the ends of the doubly oxidized binuclear unit:

$$[Ir(\mu\text{-pz})(COD)]_2 \rightarrow e^- + [Ir(\mu\text{-pz})(COD)]_2^+ \quad (6)$$

$$[Ir(\mu\text{-pz})(COD)]_2^+ \rightarrow e^- + [Ir(\mu\text{-pz})(COD)]_2^{2+} \quad (7)$$

$$[Ir(\mu\text{-pz})(COD)]_2^{2+} + 2X^- \rightarrow [Ir(\mu\text{-pz})(COD)]_2X_2 \quad (8)$$

The position and reversibility of $E_{p,a}$ for the second oxidation is very sensitive to the supporting anion and the presence of other ligands (H_2O and CH_3CN). In Table I, the position of $E_{p,a}$ for the second oxidation, $E_{1/0}^{\circ\prime}$ and $E^{\circ\prime}$ for $FeCp_2^+/FeCp_2$ as a function of the supporting anion are given. The shifts reported for $E_{p,a}$ are too large to be the result of junction potential changes. In the presence of ClO_4^-, a more coordinating anion than PF_6^-, $E_{p,a}$, occurs at +0.963 V and $i_{p,c}/i_{p,a}$ = 0.55 at ν = 100 mV/s, while in the presence of AsF_6^- $E_{p,a}$ occurs at +1.383 V. The relative stabilization of $[Ir(\mu\text{-pz})(COD)]_2^{2+}$ by X^- ($ClO_4^- > PF_6^- > AsF_6^-$) is in the order of their coordinating ability.[18] It is

(18) BF_4^-, ClO_4^-, PF_6^-, and most recently SbF_6^- have all been found to form complexes: Mayfield, H. G.; Bull, W. E. *J. Chem. Soc. A* **1971**, 2279. And: Hersh, W. H. *J. Am. Chem. Soc.* **1985**, *107*, 4599. On the basis of the acidities of HPF_6 and $HAsF_6$, the ordering of "coordination ability" should be $ClO_4^- > PF_6^- > AsF_6^-$: Clifford, A. F.; Beachell, H. C.; Jack, W. M. *J. Inorg. Nucl. Chem.* **1957**, *57*.

Scheme I. Direct 2e⁻ Transfer

$$[Ir(\mu\text{-pz})(COD)]_2 \xrightarrow{k_{het}} [Ir(\mu\text{-pz})(COD)]_2^{2+} + 2e^- \quad \text{rate determining step} \tag{10}$$

$$[Ir(\mu\text{-pz})(COD)]_2^{2+} + qCH_3CN \rightarrow [Ir(\mu\text{-pz})(COD)]_2(CH_3CN)_q^{2+} \quad \text{rapid, following step} \tag{11}$$

Scheme II. Half Regeneration

$$[Ir(\mu\text{-pz})(COD)]_2 \xrightarrow{k_{het}} [Ir(\mu\text{-pz})(COD)]_2^{+} + e^- \tag{12}$$

$$[Ir(\mu\text{-pz})(COD)]_2^{+} + qCH_3CN \rightarrow [Ir(\mu\text{-pz})(COD)]_2(CH_3CN)_q^{+} \tag{13}$$

$$[Ir(\mu\text{-pz})(COD)]_2(CH_3CN)_q^{+} + [Ir(\mu\text{-pz})(COD)]_2^{+} \rightleftharpoons [Ir(\mu\text{-pz})(COD)]_2(CH_3CN)_q^{2+} + [Ir(\mu\text{-pz})(COD)]_2 \tag{14}$$

Scheme III. Sequential 1e⁻ Transfer

$$[Ir(\mu\text{-pz})(COD)]_2 \xrightarrow{k_{het}} [Ir(\mu\text{-pz})(COD)]_2^{+} + e^- \tag{15}$$

$$[Ir(\mu\text{-pz})(COD)]_2^{+} + qCH_3CN \rightarrow [Ir(\mu\text{-pz})(COD)]_2(CH_3CN)_q^{+} \tag{16}$$

$$[Ir(\mu\text{-pz})(COD)]_2(CH_3CN)_q^{+} \xrightarrow{k_{het}} [Ir(\mu\text{-pz})(COD)]_2(CH_3CN)_q^{2+} + e^- \tag{17}$$

interesting to note that $E^{\circ\prime}_{1/0}$ for the quasi-reversible first process is nearly invariant to changes in supporting anion when allowance for junction potential changes is made. The small changes that do occur are most likely due to small changes in the relative solvation energies for the neutral, reduced form or weak, ion-pairing interactions with the unipositive, one-electron oxidized form.[8b]

The strong complexing ability of $[Ir(\mu\text{-pz})(COD)]_2^{2+}$ is further illustrated by the appearance of CV's in the presence of water. Millimolar amounts of water in these CH_2Cl_2 solutions[19] cause large shifts in the position of $E_{p,a}$ and change the chemical reversibility of the 2/1 couple. Figure 1 shows the CV of $[Ir(\mu\text{-pz})(COD)]_2$ in "moist" CH_2Cl_2/TBAH solution (1A) followed by addition of activated 4-Å molecular sieves (1B). With water in the solution, $E_{p,a}$ is shifted to less positive potentials (+0.931 V) and the coupled return peak $E_{p,c}$ is quite evident. Under these "moist" conditions, the peak current ratio $i_{p,c}/i_{p,a}$ approaches 1.0 and ΔE_p is 104 mV, suggestive of quasi-reversible behavior. As the solution is stirred and the 4-Å sieves dry the solution, $i_{p,c}$ gradually decreases and $E_{p,a}$ shifts to the position reported for "dry" conditions in Table I.

The changes in the CV produced by the presence of small amounts of water are consistent with rapid and reversible complexation of water by the two-electron oxidized form:

$$[Ir(\mu\text{-pz})(COD)]_2^{2+} + qH_2O \rightleftharpoons [Ir(\mu\text{-pz})(COD)]_2(H_2O)_q^{2+} \tag{9}$$

This description of the effect of water is favored over one that involves the catalysis of the anion complexation/decomplexation equilibrium because water effects CH_2Cl_2 solutions of the other supporting anions in a similar way and the addition of CH_3CN to CH_2Cl_2 solutions (vide infra) has an analogous effect.

$[Ir(\mu\text{-pz})(COD)]_2$ in CH_3CN Solutions. A single oxidative process is observed between 0.0 V and the solvent limit in the CV for 0.30 mM $[Ir(\mu\text{-pz})(COD)]_2$ in CH_3CN/TBAH solutions (Figure 2) at $E^{\circ\prime}$ = +0.262 V. The process shows a high degree of chemical reversibility ($i_{p,c}/i_{p,a}$ = 1.00 ± 0.05) in the range of scan rates studied. At scan rates of 100 mV/s, ΔE_p = 36 mV, much *less* than the 57 mV expected for a Nernstian 1 e⁻ electrode process. An LSV scan obtained at the RDE for a 0.27 mM CH_3CN/TBAH solution (ν = 1 mV/s and ω = 10.47 rad/s) is shown in Figure 3B. The plot of E vs. log $\{i_{c,l} - i)/(i - i_{a,l})\}$ for this LSV ($E_{applied}$ > +0.22 V) has a slope of +0.046 V and an intercept of +0.260 V. The magnitude of the slope is consistent with a net two-electron electrode process.

Chronocoulometry experiments conducted on 0.27 mM solutions with a potential step from +0.0 to +0.5 V gave a linear Anson plot with a slope of 14.7 $C/s^{1/2}$ for a 1.0-s step. From this slope, a $nD^{1/2}$ value of 7.1 × 10^{-3} $cm/s^{1/2}$ is obtained. The Stokes–Einstein equation predicts[17] a value of D for CH_3CN solutions of 1.25 × 10^{-5} cm^2/s. With the assumption that n = 2, an experimental value of D of 1.26 × 10^{-5} cm^2/s is calculated, in excellent agreement with the theoretical estimate.

Bulk electrolysis (BE) of the orange CH_3CN solution results in a color change to yellow with concomitant removal of two electrons per $[Ir(\mu\text{-pz})(COD)]_2$ unit. Addition of slightly more than 2 equiv of benzyltriethylammonium chloride to the yellow solution results in an instantaneous color change to a yellow–brown solution, which has identical UV–vis spectral features to the previously characterized[10] binuclear Ir(II) compound $[Ir(\mu\text{-pz})(COD)Cl]_2$.

All of these experiments are consistent with the occurrence of a net 2e⁻ oxidation of $[Ir(\mu\text{-pz})(COD)]_2$ in acetonitrile solutions on the CV, CC, and BE time scales. Several different mechanisms can lead to the observation of a net two-electron process in CV, CC, LSV–RDE, and BE experiments, but only mechanisms consistent with the experimental data need be considered. Mechanisms[20] that meet these criteria are direct two-electron transfer at the electrode (E), first-order half regeneration (EC), and two sequential, one-electron transfers with an interceding chemical step (ECE). The most likely nuances of these possible mechanisms are outlined in Schemes I–III, with step 13 first-order and rate-determining.

The invariance of the CC n value of 2 over the range of step-times available with our equipment (20 ms to 1 s) requires that any reactions preceding or at the rate-limiting step are fast on the millisecond time scale. The n value of 2 also rules out mechanisms that are second-order with respect to $[Ir(\mu\text{-pz})(COD)]_2^{+}$ or its complexes.[21] Specifically, a rate-determining step involving the classical second-order disproportionation of the form

$$2[Ir(\mu\text{-pz})(COD)]_2^{+} \rightarrow [Ir(\mu\text{-pz})(COD)]_2 + [Ir(\mu\text{-pz})(COD)]_2^{2+} \tag{18}$$

(19) The solubility of water in dichloromethane is reported to be 0.24% by weight at 20 °C (Burdick & Jackson Solvent Guide). This represents an approximately 0.18 M solution. Our "moist" solutions have water concentrations well below this concentration.

(20) E = electrochemical step; C = chemical step. By example, an ECE mechanism then is ($A \xrightarrow{(E)} e^- + A^+ \xrightarrow{(C)} B^+ \xrightarrow{(E)} B^{2+} + e^-$). A brief discussion of the effect chemical reactions have on CV and CC experiments may be found in: Bard, A. J.; Faulkner, L. R. *Electrochemical Methods*; Wiley: New York, 1980; pp 429–485. Two papers that discuss the effect of EC and ECE mechanisms on CV experiments have been published: Nadjo, L.; Saveant, J. M. *Electroanal. Chem. Interfacial Electrochem.* **1973**, *48*, 113. Mastragostino, M.; Nadjo, L.; Saveant, J. M. *Electrochim. Acta* **1978**, *13*, 721.

(21) Fractional n values are obtained in CC experiments for ECE mechanisms where the rate-limiting step for the transfer of the second electron is controlled by a second-order process. In this case $n \approx 1.75$; see: Feldberg, S. W. In *Electroanalytical Chemistry*; Bard, A. J., Ed.; Marcel Dekker: New York, 1969; Vol. III, p 199.

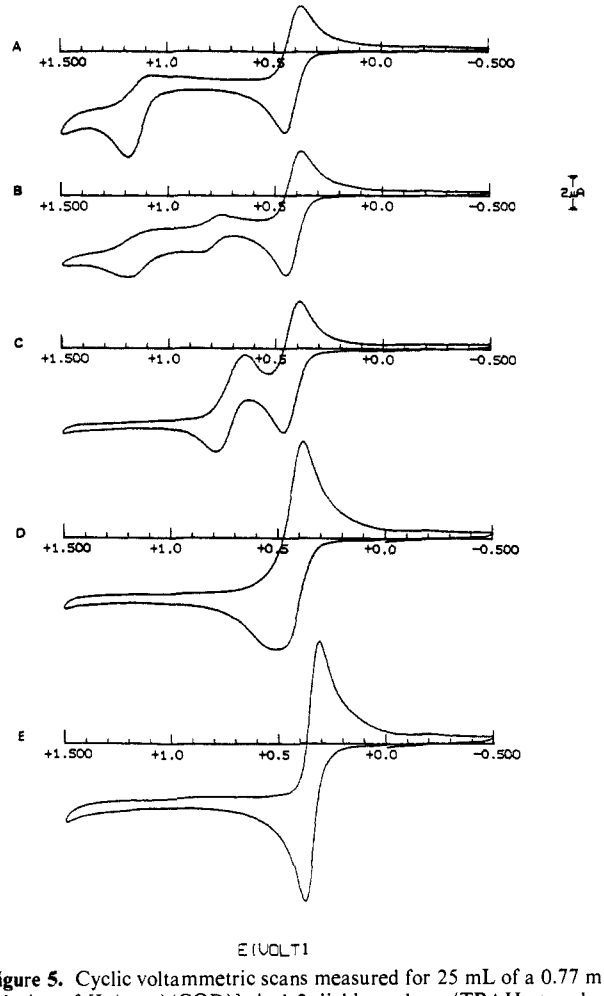

Figure 5. Cyclic voltammetric scans measured for 25 mL of a 0.77 mM solution of $[Ir(\mu\text{-pz})(COD)]_2$ in 1,2-dichloroethane/TBAH at a glassy carbon electrode. All cyclic voltammograms were recorded at 20 mV/s: (A) 0 μL of added CH_3CN/TBAH; (B) 10 μL of added 0.76 M CH_3CN/TBAH; (C) 2 μL of added neat CH_3CN/TBAH; (D) 100 μL of added neat CH_3CN/TBAH; (E) 2100 μL of added neat CH_3CN/TBAH.

is ruled out.

The electrochemical data are compatible with all three schemes, but mechanisms analogous to Scheme I (direct $2e^-$ transfer) have not been verified for other systems. The differentiation of the remaining two schemes requires additional experimental results.

$[Ir(\mu\text{-pz})(COD)]_2$ in Mixed CH_2Cl_2/CH_3CN Solutions. Addition of CH_3CN to CH_2Cl_2 solutions of $[Ir(\mu\text{-pz})(COD)]_2$ causes an interesting series of changes to occur in the CV experiment. We identify three distinct sets of CV behavior as illustrated in Table II.

Case A. The stepwise addition of subequivalent amounts of CH_3CN to a 4.94 mM solution of $[Ir(\mu\text{-pz})(COD)]_2$ in CH_2Cl_2 results in the behavior labeled A in Table II. With each addition of CH_3CN to the solution, $E_{p,a}$ at +1.28 V for the second chemically irreversible oxidation gradually decreases in intensity and a new, quasi-reversible wave grows into the CV with $E_{p,a}$ at +0.849 V at ν = 100 mV/s. An analogous change occurs in DCE/TBAH solutions as illustrated in Figure 5A and 5B. This behavior is indicative of strong, reversible complexation of the two-electron oxidized binuclear complex:

$$[Ir(\mu\text{-pz})(COD)]_2^{2+} + pCH_3CN \rightleftharpoons [Ir(\mu\text{-pz})(COD)]_2(CH_3CN)_p^{2+} \quad (19)$$

With the assumption that the peak current, i_a, of the new wave is a measurement of the concentration of complexed, two-electron oxidized binuclear species, the ratio of complexed to uncomplexed two-electron oxidized binuclear can be determined as a function of free $[CH_3CN]$.

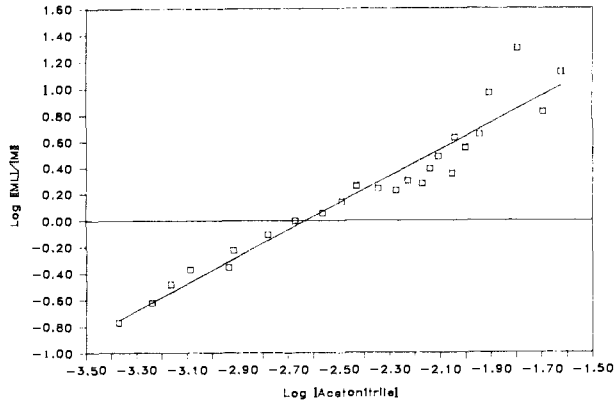

Figure 6. Plot of log {[complexed]/[uncomplexed]} vs. log $[CH_3CN]$ for the sequential addition of 1.9 M CH_3CN/TBAH in CH_2Cl/TBAH to a 4.94 mM solution of $[Ir(\mu\text{-pz})(COD)]_2$ in CH_2Cl_2/TBAH. $i_{p,a}$ for the complexed form of $[Ir(\mu\text{-pz})(COD)]_2^{2+}$ was used to compute [complexed]/[uncomplexed] (see Experimental Section). Cyclic voltammetric data were obtained at ν = 100 mV/s. Experimental points are presented as squares. The least-squares line has slope = 1.02 and intercept = 2.68.

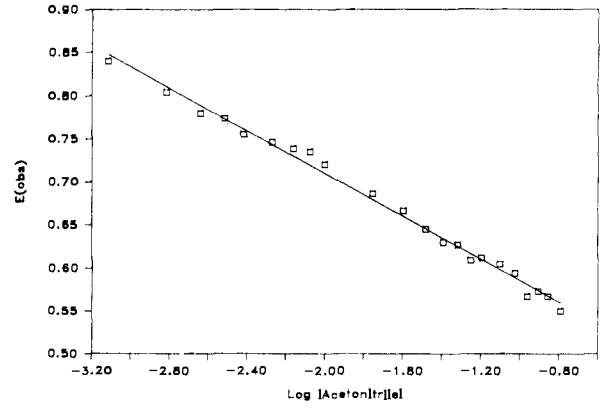

Figure 7. Plot of $E_{p,a}^{2/1}$ vs. log $[CH_3CN]$ for the sequential addition of CH_3CN to a 0.55 mM solution of $[Ir(\mu\text{-pz})(COD)]_2$ in CH_2Cl_2/TBAH. Cyclic voltammetric data were obtained at ν = 50 mV/s. Experimental points are represented as squares. The least-squares line has slope = −0.124 V and intercept = +0.462 V.

The plot (eq 1) of log {[complexed]/[uncomplexed]} vs. log $\{[CH_3CN]_{added} - p[complexed]\}$ (Figure 6) gives an excellent straight line with a slope of 1.02 and intercept of 2.68. The slope gives directly the value for p in equilibrium 19. The intercept is then equal to log K_1 = 2.68 ($K_1 \approx 480\ M^{-1}$). Perhaps most importantly, the quasi-reversible nature of the wave involving the complexed two-electron oxidized form and the determination of K_1 for equilibrium 19 enables an estimate of the $E_{2/1}{}^{\circ\prime}$ of +0.98 V to be made for eq 20.

$$e^- + [Ir(\mu\text{-pz})(COD)]_2^{2+} \rightleftharpoons [Ir(\mu\text{-pz})(COD)]_2^{+} \quad (20)$$

Case B. The results of further sequential additions of CH_3CN aliquots to the 0.77 mM solution of $[Ir(\mu\text{-pz})(COD)]_2$ in 1,2-dichloroethane/TBAH are shown in Figure 5C–5E (ν = 20 mV/s). Addition of CH_3CN (Figure 5C: 2μL of added CH_3CN) causes the wave due to the more positive electrode process to shift to more negative potentials, while the first wave does not shift. Further microliter additions of CH_3CN to the solution cause the more positive wave to shift until it overtakes and merges (Figure 5D: 100 μL of added CH_3CN) with the first wave, to give a single wave (case C) with ΔE_p = 126 mV, and peak currents larger than for either of the two, one-electron waves observed in neat 1,2-dichloroethane/TBAH. Further additions of CH_3CN cause the merged wave to sharpen (Figure 5E: ΔE_p = 75 mV at added CH_3CN = 2100 μL) and continue the shift to more negative potentials.

Analysis of more extensive CV data obtained for a sequential addition experiment with CH_2Cl_2 as the solvent for the $[CH_3CN]$

range where two discrete waves are present was made according to eq 5 (Experimental Section). The plot of $E_{p,a}$ for the second wave vs. log [CH_3CN] is shown in Figure 7. This plot gives a straight line (correlation coefficient = 0.9787, slope = −0.124 V, and intercept = +0.462 V). The slope of this line is indicative of the overall reversible binding of 2.1 ± 0.1 CH_3CN ligands to the *two*-electron oxidized binuclear complex, because the *one*-electron oxidized complex does not bind CH_3CN to an appreciable extent.

$$[Ir(\mu\text{-pz})(COD)]_2^{2+} + 2CH_3CN \rightleftharpoons [Ir(\mu\text{-pz})(COD)(CH_3CN)]_2^{2+} \quad (21)$$

The intercept value gives the total, relative stabilization of the two-electron oxidized form relative to the one-electron oxidized form in 1 M CH_3CN vs. pure CH_2Cl_2/TBAH. The largest contribution to the intercept value is stabilization of $[Ir(\mu\text{-pz})(COD)]_2^{2+}$ via the complexation equilibrium 21. Other contributions to the intercept value include changes in relative solvation energies and, to a lesser extent, small changes (~10 mV) in junction potential. An independent measurement of these effects would be needed to extract log K_1K_2 from the intercept value. When the derived value for $E^{\circ\prime}_{2/1}$ of +0.98 V and the intercept value (+0.462 V) are utilized, the net stabilization of $[Ir(\mu\text{-pz})(COD)]_2^{2+}$ in 1 M CH_3CN in CH_2Cl_2/TBAH compared with neat CH_2Cl_2/TBAH is 0.518 V or 11.9 kcal/mol.

Case C. After the free concentration of CH_3CN reaches about 2.0 M, two separate waves are no longer observed. As [CH_3CN] is increased, the combined wave sharpens and continues to shift toward negative potentials. The sequential addition data in the CH_3CN concentration range 2–19 M were not analyzed quantitatively because the shifts are of the same magnitude as the change in junction potential.

Conclusions

In the poorly coordinating solvent CH_2Cl_2, two thermodynamically discrete le^- processes are observed for the oxidation of $[Ir(\mu\text{-pz})(COD)]_2$. The first wave is quasi-reversible with an $E^{\circ\prime}$ value that is independent of the supporting electrolyte and the presence of water. The second wave is chemically irreversible in dry CH_2Cl_2/TBAH, partially chemically reversible in CH_2Cl_2/TBAP, and chemically reversible in "moist" CH_2Cl_2/TBAH. Bulk electrolyses in CH_2Cl_2 solutions at potentials positive of the first oxidation yield n values of two even though n for the electrode reaction is one under these conditions. The initially produced radical $[Ir(\mu\text{-pz})(COD)]_2^+$ undergoes a slow reaction with CH_2Cl_2 that yields a two-electron oxidative addition product. Addition of subequivalent amounts of acetonitrile to dichloromethane solutions of $[Ir(\mu\text{-pz})(COD)]_2$ results first in the growth of a new quasi-reversible wave ($E_{p,a}$ at +0.849 V) and in the simultaneous disappearance of the irreversible wave ($E_{p,a}$ = +1.28 V). When sufficient amounts of acetonitrile are added to cause the disappearance of the irreversible wave, the new wave shifts to less positive potentials due to the formation of $[Ir(\mu\text{-pz})(COD)]_2(CH_3CN)_2^{2+}$.

In pure CH_3CN solutions, the concentration of acetonitrile is sufficient to shift the $E^{\circ\prime}_{2/1}$ couple to potentials negative of the $E^{\circ\prime}_{1/0}$ formal potential. Under these conditions, a single process is observed in the CV, and the bulk electrolysis and electrode reaction n values are both 2.0 e^-/binuclear unit. This result contrasts two different reports in the literature[22,23] from limited CV results that claim n = 1 for the oxidation of $[Ir(\mu\text{-pz})(COD)]_2$ in CH_3CN solutions. In view of the sensitivity of the electrochemical response of the $[Ir(\mu\text{-pz})(COD)]_2$ system to medium effects and the presence of small amounts of water, the previous difficulty in determining the mechanistic details of this system is apparent.

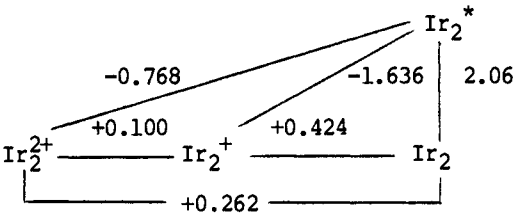

Figure 8. Modified Latimer diagram that illustrates one- and two-electron, ground- and excited-state processes. See ref 24 for details.

Although extrapolation of these results to the photochemical oxidations of $[Ir(\mu\text{-pz})(COD)]_2$ is perhaps speculative, we believe our results may have important implications concerning the thermodynamics of nearly simultaneous two-electron transfers from the lowest excited state of $[Ir(\mu\text{-pz})(COD)]_2$ to suitably designed two-electron acceptors. The electrochemical data allow us to construct a modified Latimer diagram[24] (Figure 8) for $[Ir(\mu\text{-pz})(COD)]_2$ in CH_3CN solutions that include two-electron processes. Because the electron-transfer kinetics of a one-step, two-electron transfer from Ir_2* may be slow,[5] rapid sequential one-electron transfers during the lifetime of a single solvent cage may prove to be the more kinetically favored pathway for the net two-electron reduction of an acceptor by Ir_2*. This "kinetic" view would place an additional thermodynamic constraint on net two-electron transfer reactions of Ir_2*. A negative free energy for the second electron transfer may be required to complete the sequence leading to net, two-electron transfer. As in the case of one-electron excited-state electron transfers, escape from the solvent cage will be required to observe the transient products of the net reaction. The further experimental exposition of these ideas is currently being pursued in our laboratory.

Acknowledgment. We thank John Evans and Harry B. Gray for helpful discussions. Johnson-Matthey Inc. is acknowledged for a generous loan of $IrCl_3 \cdot 3H_2O$.

Supplementary Material Available: Experimental data for the sequential additions of CH_3CN to CH_2Cl_2 solutions of $[Ir(\mu\text{-pz})(COD)]_2$ (Tables 1 and 2) (2 pages). Ordering information is given on any current masthead page.

(22) Marshall, J. L.; Stobart, S. R.; Gray, H. B. *J. Am. Chem. Soc.* **1984**, *106*, 3027.

(23) Bushnell, G. W.; Fjeldsted, D. O. K.; Stobart, S. R.; Zaworotko, M. J.; Knox, S. A. R.; Macpherson, K. A. *Organometallics* **1985**, *4*, 1107.

(24) Ir_2 is used as the abbreviation for $[Ir(\mu\text{-pz})(COD)]_2$. The Latimer diagram is constructed without junction potential corrections. The potential for the $2e^-$ reduction of Ir_2^{2+} is taken as the $E^{\circ\prime}$ measured in neat CH_3CN/TBAH solution. $E^{\circ\prime}$ for the Ir_2^{2+}/Ir_2^+ couple in CH_3CN was estimated from $E^{\circ\prime}_{2/1} \approx 2E^{\circ\prime}_{2/0} - E^{\circ\prime}_{1/0}$ (CH_2Cl_2) = 2(0.262) − (0.424) = 0.100 V. Excited state potentials were calculated in a manner analogous to ref 22.

(25) Simultaneous two-electron transfers have been the subject of a theoretical investigation; see: Gurnee, E. F.; Magee, J. L. *J. Chem. Phys.* **1957**, *26*, 1237.